

VARIABILITY OF THE CENTIMETER-SUBMILLIMETER SPECTRUM AND POLARIZATION OF 3C 273 DURING OUTBURST

J. A. STEVENS,¹ E. I. ROBSON,² AND W. K. GEAR¹

Joint Astronomy Centre, 660 North A‘ohökü Place, University Park, Hilo, Hawaii 96720

T. V. CAWTHORNE

Centre for Astrophysics, University of Central Lancashire, Preston PR1 2HE, UK

M. F. ALLER AND H. D. ALLER

Astronomy Department, University of Michigan, Ann Arbor, MI 48109-1090

H. TERÄSRANTA

Metsähovio Radio Research Station, Metsahovintie, SF-02540 Kylmäla, Finland

AND

M. C. H. WRIGHT

Radioastronomy Laboratory, University of California, Berkeley, CA 94720

Received 1997 September 9; accepted 1998 March 2

ABSTRACT

Centimeter to submillimeter total flux and polarization monitoring data are used to investigate the nature of a prominent flare in the quasar 3C 273 during 1995/6. After removal of the quiescent level, the resulting “flare spectra” are well fitted by a simple homogeneous synchrotron source model, which in turn allows the movement of the self-absorption turnover to be tracked during the flare. Both the flare amplitude/time delay relationship and the overall spectral evolution are qualitatively consistent with existing models. The early evolution of the spectrum is best determined and is shown to be in excellent agreement with the Compton stage of the Marscher & Gear shock model. However, the polarization behavior during the flare is different at millimeter and centimeter wavelengths and the observations are difficult to reconcile with a simple transverse shock. They are, however, consistent with a conical shock for which the observed polarization properties vary with distance along the jet. Such variations may be caused, for example, by a change in cone angle owing to disruption caused by the growing component of the magnetic field parallel to the jet axis or by a moderate change in viewing angle.

Subject headings: galaxies: jets — polarization — quasars: general — quasars: individual (3C 273) — radio continuum: galaxies

1. INTRODUCTION

The quasar 3C 273 is a well-studied source at all wavelengths. On milliarcsecond (mas) scales its radio components display superluminal speeds (Unwin et al. 1985), which, together with rapid multifrequency variability (e.g., Robson et al. 1983; Courvoisier et al. 1988; Aller et al. 1985; McNaron-Brown et al. 1997), has led to its classification as a blazar. The broadband continuum energy spectrum (νS_ν) of 3C 273 displays components peaking at mid-IR, UV, and low-energy γ -ray wavelengths (e.g., Lichti et al. 1995). This work is concerned with the centimeter–submillimeter emission from the first of these components. At these wavelengths the observed flux is synchrotron radiation from the base of the relativistic jet, and the spectra often show the turnover characteristic of self-absorption (e.g., Gear et al. 1994).

Observations of the flux and polarization variability of 3C 273 (e.g., Robson et al. 1983) and other blazars, such as BL Lacertae (Aller et al. 1985), have provided evidence that the “flares” in these sources are produced by shock waves that propagate along the relativistic jet (e.g., Marscher & Gear 1985; Lind & Blandford 1985; Hughes, Aller, & Aller 1985, 1989a, 1989b). At frequencies above ~ 90 GHz (3.3

mm) such monitoring data enable studies of the radio jets on scales that are currently inaccessible to VLBI, thus providing the only means of investigating the early stages of flare evolution (e.g., Stevens et al. 1994).

During late 1995 and early 1996, 3C 273 produced a prominent flare at millimeter and submillimeter wavelengths that subsequently propagated to the radio part of the spectrum. In this paper the spectral and polarization variability during the flare are analyzed, the main motivation being to investigate the extent to which the data are consistent with the shocked-jet hypothesis.

2. OBSERVATIONS

Millimeter and submillimeter monitoring data have been collected at the James Clerk Maxwell Telescope (JCMT) since 1989 at 670, 375, 270, 230, and 150 GHz (0.45, 0.8, 1.1, 1.3, and 2.0 mm, respectively). Recent observations have included data at 400 and 345 GHz (0.75 and 0.85 mm) rather than at 375 GHz in order to avoid the strong atmospheric water line in this region. Of the 17 sources monitored, 3C 273 is one of the better sampled, and a previous paper has discussed the data up to and including 1992 (Robson et al. 1993). Most of the data were taken with the common-user bolometer UKT14 (Duncan et al. 1990), and the observing techniques and data reduction procedures are discussed by Robson et al. (1993) and by Stevens & Robson (1994). A single 230.5 GHz measurement was made on 1996 June 1 with a heterodyne instrument in continuum mode,

¹ Also at Mullard Space Science Laboratory, University College London, Holmbury St. Mary, Dorking, Surrey RH5 6NT, UK.

² Also at Centre for Astrophysics, University of Central Lancashire, Preston PR1 2HE, UK.

which measures the total power. The calibration was identical to that employed with the continuum instrument.

Data at frequencies close to 90 GHz are from the Berkeley-Illinois-Maryland Array (BIMA) at Hat Creek, California. The flux densities are calibrated from observations of the planets using surface brightness values given by Ulich (1981).

The 37 and 22 GHz data are from Metsähovi Radio Research Station, Finland (see Teräsraanta et al. 1992), while observations at 14.5, 8.0, and 4.8 GHz are from the University of Michigan Radio Astronomy Observatory (UMRAO; see Aller et al. 1985). These observatories have dedicated monitoring facilities and provide excellent coverage.

3. RESULTS

3.1. The Light Curves

The multifrequency light curves for the period 1994–1997 are shown in Figure 1, where only the best-sampled JCMT wavelengths are included. At frequencies of 90 GHz and higher, the most prominent feature is the large flare peaking at the end of 1995 (hereafter, the 1995 flare). This flare is also apparent on the 37–8.0 GHz light curves, but with increasing time delay with respect to the higher frequencies. For comparison with model predictions, Table 1 gives the flare amplitudes and time delays between different frequencies for the 1995 flare. The amplitudes are simply the difference between maximum and minimum flux levels. Time delays were estimated with application of the discrete correlation function (DCF; Edelson & Krolik 1988) and the interpolated correlation function (ICF; Gaskell & Peterson 1987). The entire data trains were used for time delay determination. Figures 2 and 3 show the resulting correlations between the best-sampled high-frequency light curve (270 GHz) and those at lower frequencies. Litchfield, Robson, & Hughes (1995) have discussed in some detail the application of these methods to blazar light curves, but in particular, it should be noted that the ICF performs more satisfactorily on the least well-sampled data streams (Peterson 1993 and references therein). This finding is evident from inspection of Figure 2: the DCF produces noisy results for the first three panels (270 GHz versus 230, 150, and 90 GHz), whereas the ICF is smoother and single peaked. For the better sampled data streams, the two techniques give very similar results, but, particularly at low frequencies, the absolute value of the lag is difficult to determine because of the broadening of

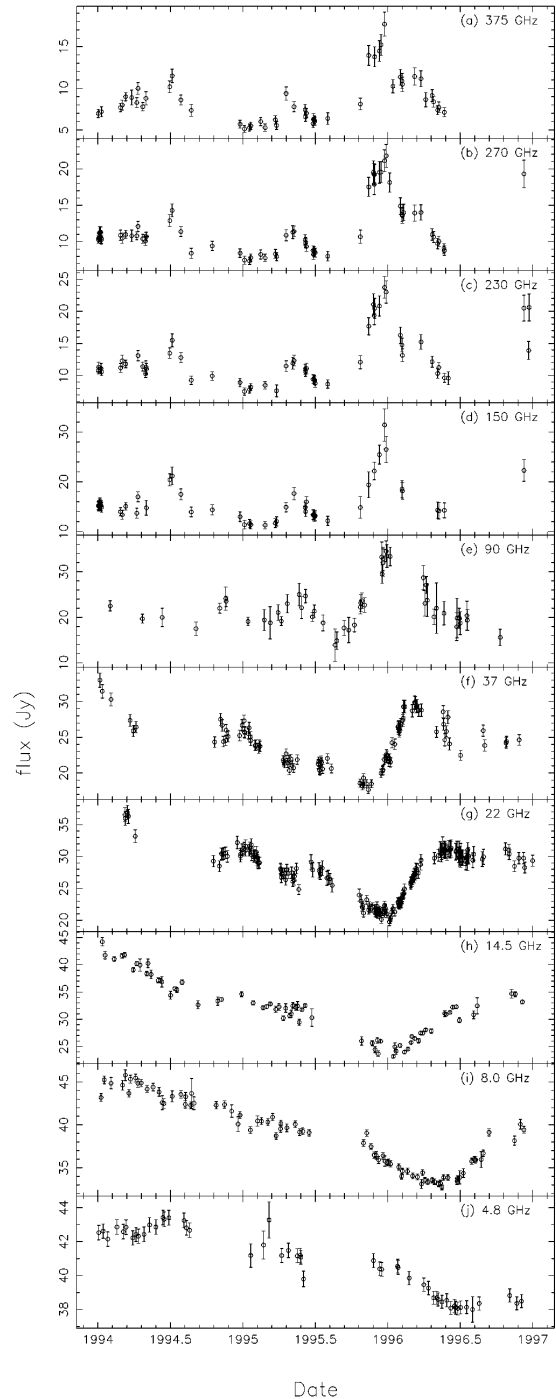


FIG. 1.—Submillimeter–centimeter (375–4.8 GHz) light curves of 3C 273 from 1994–1997. Note the prominent flare in the millimeter regime during late 1995 and its subsequent evolution to longer wavelengths.

TABLE 1

FLARE AMPLITUDES AND TIME DELAYS FOR THE 1995 FLARE

Frequency (GHz)	Flare Amplitude (Jy)	Time Delay (days)
375	12.6	0
270	14.4	...
230	16.2	0
150	20.1	0
90	20.6	0–20
37	12.2	80
22	12.1	160
14.5	11.5	200–400
8.0	7.3	300–500
4.8	>400

NOTE.—The time delays are all with respect to the 270 GHz light curve.

the flare and, in some cases, the sparse sampling close to the flare peak. At the very lowest frequencies (4.8 and possibly 8.0 GHz), the flare does not even reach its maximum. In these cases a range of probable lags or a lower limit is given in Table 1. It should be noted that the precise value of the time delay is not required for comparison with the model (see § 4).

The amplitudes grow between 375 and 150 GHz, and no time delays are observed between these light curves. There may then be a small plateau in flare amplitude between 150 and 90 GHz, with a correspondingly small time delay of 20

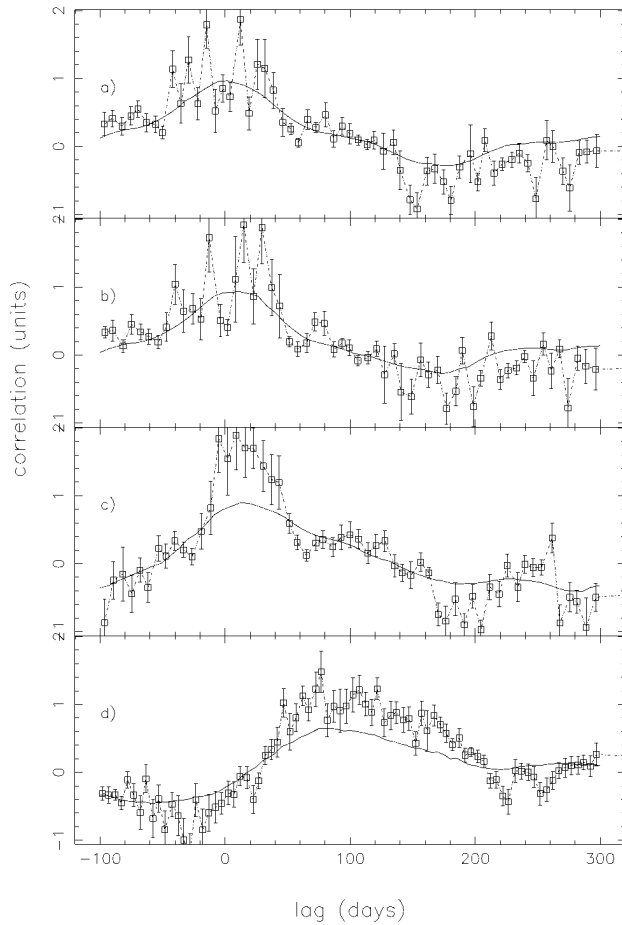


FIG. 2.—Application of the DCF (points and dotted line) and ICF (solid line) between the 270 GHz and (a) 230, (b) 150, (c) 90, and (d) 37 GHz light curves.

days. At frequencies below 90 GHz, the amplitudes drop off, and increasing time delays are apparent between the light curves.

3.2. Polarization Observations

The polarization data will be discussed in relation to the milliarcsecond-scale VLBI jet, which at 10.7 GHz (2.8 cm) has a position angle of approximately 230° (e.g., Cohen et al. 1987) and at 100 GHz (3 mm) has a position angle of about 240° (Bååth et al. 1991).

The 270 GHz polarization of 3C 273 has been measured on 10 occasions between 1989 and 1996 at the JCMT (Nartallo et al. 1998). The major results from these observations are the following: (1) The polarization is low during quiescent periods—during 1992, when the flux at millimeter wavelengths was relatively low (see Stevens et al. 1994), the 270 GHz polarization was typically only 0.7%–1.4%. (2) During flares the polarization is higher—for example, during the 1995 flare, the polarization was 6%–7%. (3) For all except the lowest polarization measurement, the electric field vector was observed to be perpendicular to the VLBI jet axis. Taken together, points (1) and (2) produce the correlation of polarization with flux density reported by Nartallo et al. (1998).

At centimeter wavelengths (the 14.5 GHz data are the most revealing; see Fig. 4) we find that (4) during quiescent periods the polarization is typically $\sim 6\%$. (5) During flares the polarization is lower, but not hugely so, with typical

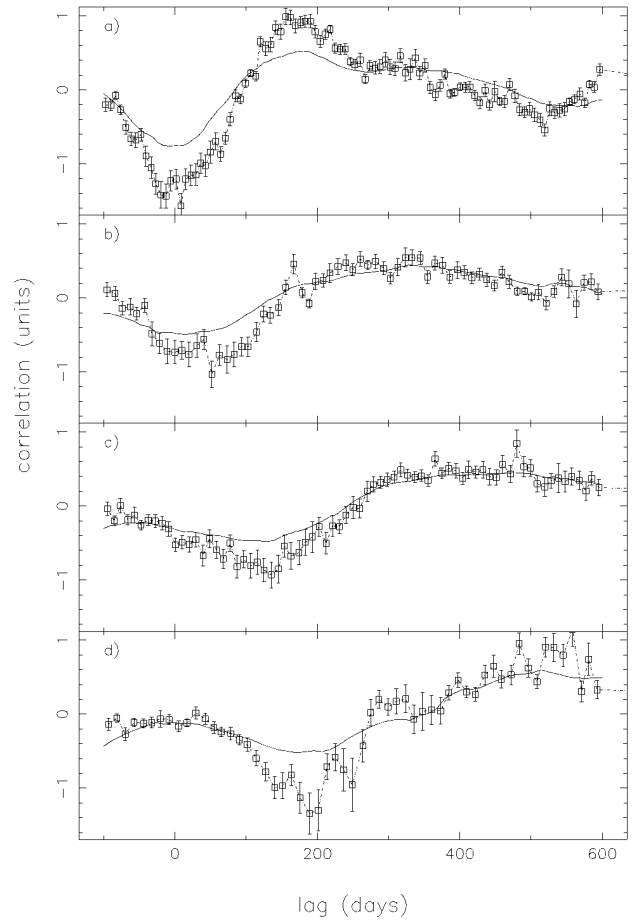


FIG. 3.—Application of the DCF (points and dotted line) and ICF (solid line) between the 270 GHz and (a) 22, (b) 14.5, (c) 8.0, and (d) 4.8 GHz light curves.

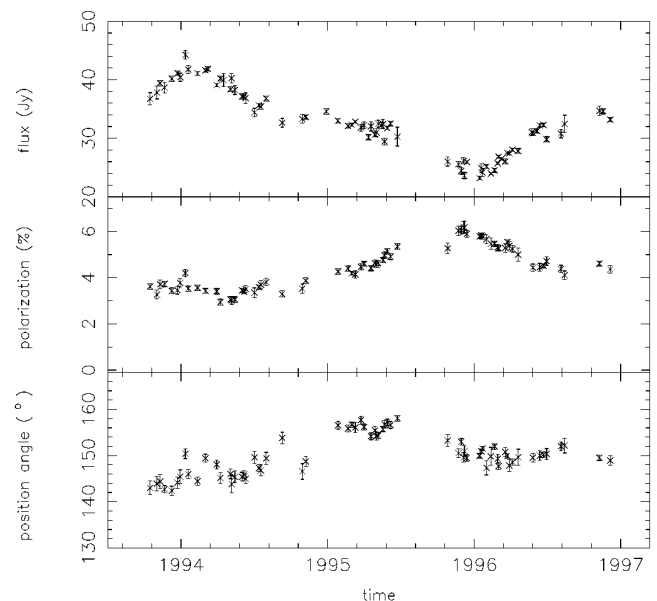


FIG. 4.—14.5 GHz flux, polarization, and position angle monitoring data from UMRAO. Note how the flux and polarization are anti-correlated. The structural position angle of the VLBI jet is between 230° and 240° , and so polarization position angles of 140° – 150° correspond to perpendicular alignment of the electric vector.

values of 3%–4%. (6) The polarization position angle suggests that the electric vector is aligned perpendicular to the VLBI jet structural axis at all epochs, similar to what was found at millimeter wavelengths. Points (4) and (5) suggest that at centimeter wavelengths the flux and polarization are anticorrelated, the opposite of what was found at 270 GHz. Additionally, the polarization of the underlying jet is higher at centimeter wavelengths than at millimeter wavelengths.

3.3. Spectral Shape and Evolution

Important clues to the origin of the flares in radio-loud active galaxies can be gained by studying the shape and

evolution of the spectrum during the outburst. It is first necessary to subtract the emission from the underlying jet, which is assumed to be steady or only slowly variable. The last point appears to hold well for 3C 273, since inspection of the light curves shows that the source returned to approximately the same low-level fluxes as for 1988–1990 (Robson et al. 1993). The 670–22 GHz quiescent spectrum presented in that paper is thus adopted here. At frequencies lower than 22 GHz, the adopted quiescent flux is simply the lowest datum. The previous outburst is typically still decaying at low frequencies, and so these values may not define the true quiescent level but rather a “preflare” level.

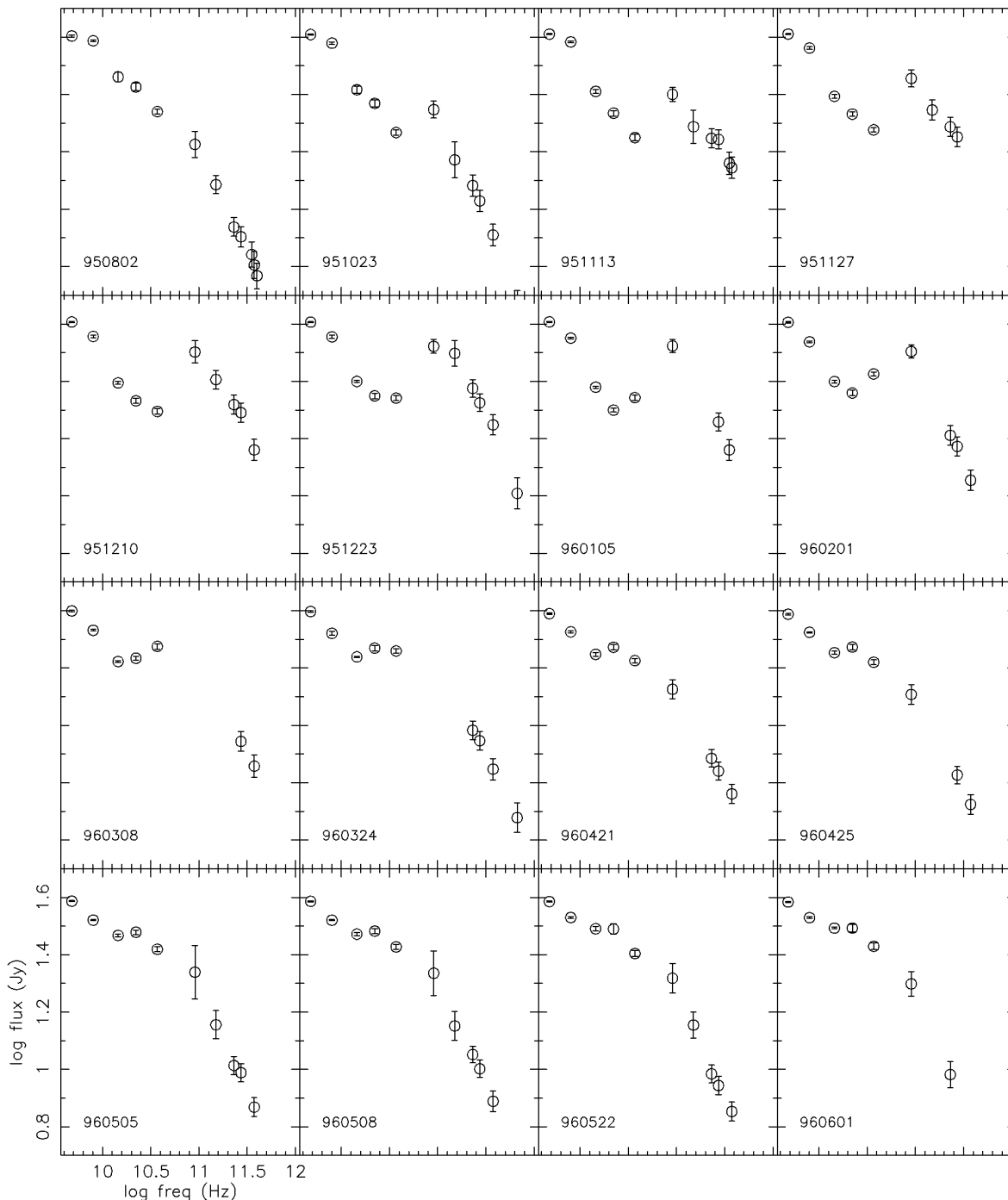


FIG. 5.—Quasi-simultaneous linearly interpolated spectra of 3C 273. The date on the panels refers to the epoch of the JCMT observations.

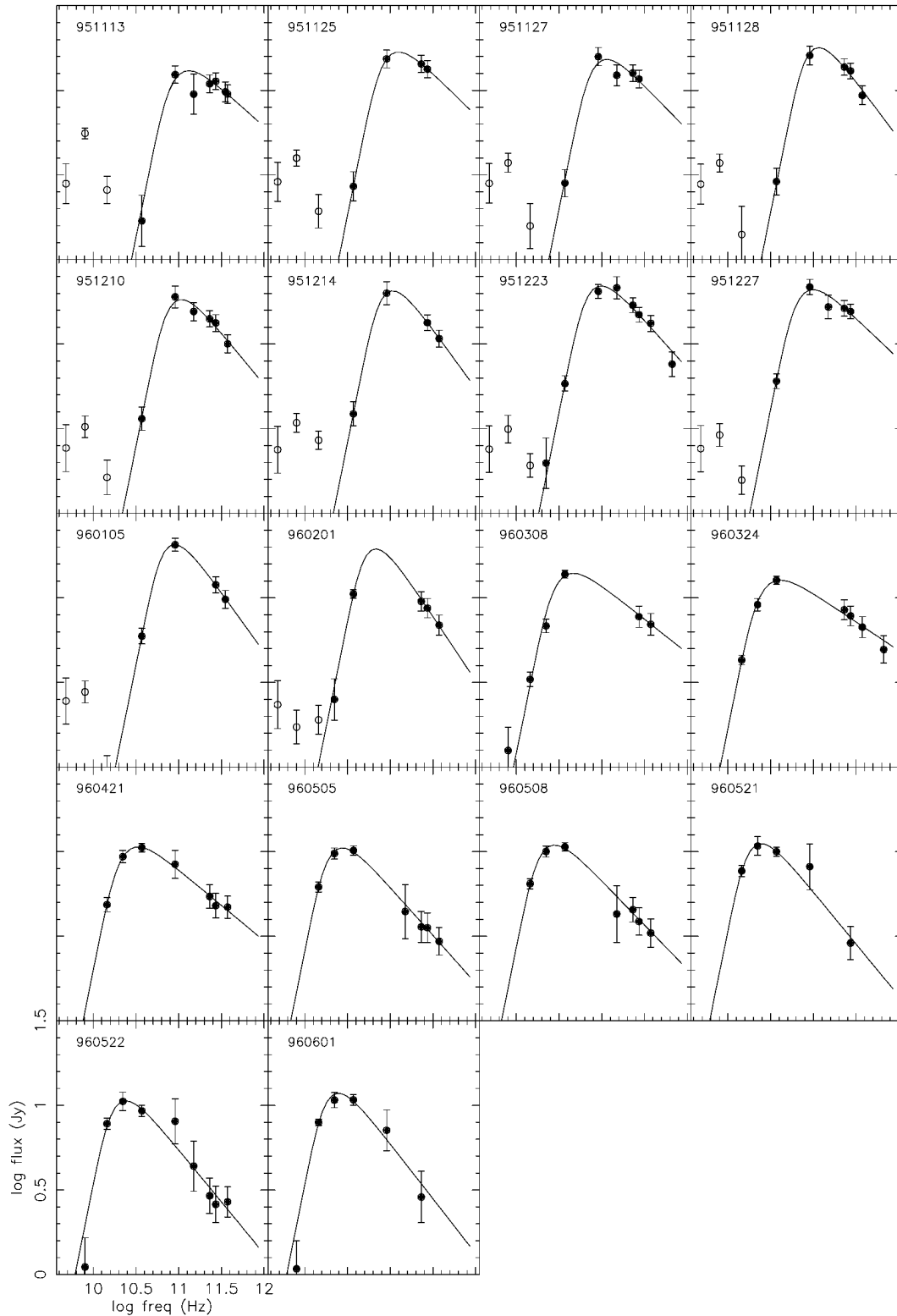


FIG. 6.—Quiescent subtracted or flare spectra. The fits (to filled symbols only) are homogeneous synchrotron spectra.

Figure 5 shows a sequence of composite spectra (no subtraction) for late 1995 and early 1996, a period commensurate with the 1995 flare and also with the unusual polarization behavior described above. These spectra were constructed by selecting dates on which JCMT data were available, then linearly interpolating the better sampled

lower frequency light curves, taking care to avoid large gaps in the coverage. The spectra are discussed briefly below.

The first panel from 1995 August shows an almost smooth spectrum between 4.8 and 400 GHz (750 μm), although there are one or two slight discontinuities that are most likely related to the small flare at JCMT frequencies

TABLE 2
PARAMETERS FROM HOMOGENEOUS SYNCHROTRON CURVE
FITS TO THE QUIESCENT SUBTRACTED (FLARE)
SPECTRA OF 3C 273

Date (1)	$\log \nu_m$ (Hz) (2)	$\log S_m$ (Jy) (3)	s (4)	α (5)
131195.....	11.12	1.116	1.90	-0.45
251195.....	11.10	1.226	1.99	-0.50
271195.....	11.06	1.183	2.05	-0.53
281195.....	11.06	1.252	2.36	-0.68
101295.....	11.03	1.263	2.22	-0.61
141295.....	11.03	1.315	2.39	-0.70
231295.....	10.99	1.344	2.13	-0.57
271295.....	11.00	1.322	1.96	-0.48
050196.....	10.95	1.315	2.40	-0.70
010296.....	10.83	1.289	2.51	-0.76
080396.....	10.67	1.145	1.80	-0.40
240396.....	10.61	1.105	1.68	-0.34
210496.....	10.52	1.027	1.84	-0.42
050596.....	10.44	1.022	2.13	-0.57
080596.....	10.45	1.039	2.05	-0.52
210596.....	10.39	1.047	2.23	-0.61
220596.....	10.38	1.027	2.23	-0.61
010696.....	10.39	1.071	2.30	-0.65

during early-mid 1995 and its subsequent time-lagged evolution. The next eight panels correspond to the rise of the 1995 flare; here the spectrum shows at least two components, one peaking at the lowest frequency, which probably represents the decay of a previous event, and a second peaking at around 90 GHz. The remaining panels show the evolution of this second peak to lower frequencies.

Figure 6 shows the result of quiescent subtraction on the composite spectra described above. Spectra constructed on dates prior to 1995 November 13 could not be fitted, because the flare flux was only marginally “detected” after quiescent subtraction, i.e., the data were too noisy. Note also that Figure 6 includes all spectra that could be fitted, whereas, for brevity, Figure 5 omits epochs closely spaced in

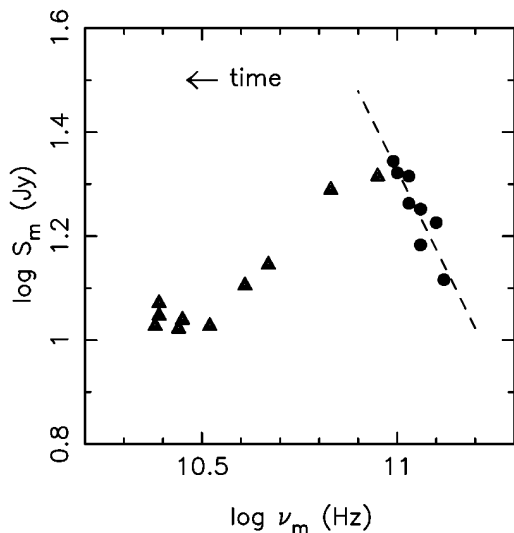


FIG. 7.—Evolution of peak flux (S_m) with peak frequency (ν_m). The dashed line is a “fit” to the first eight points (*filled circles*) and has a slope of -1.5 .

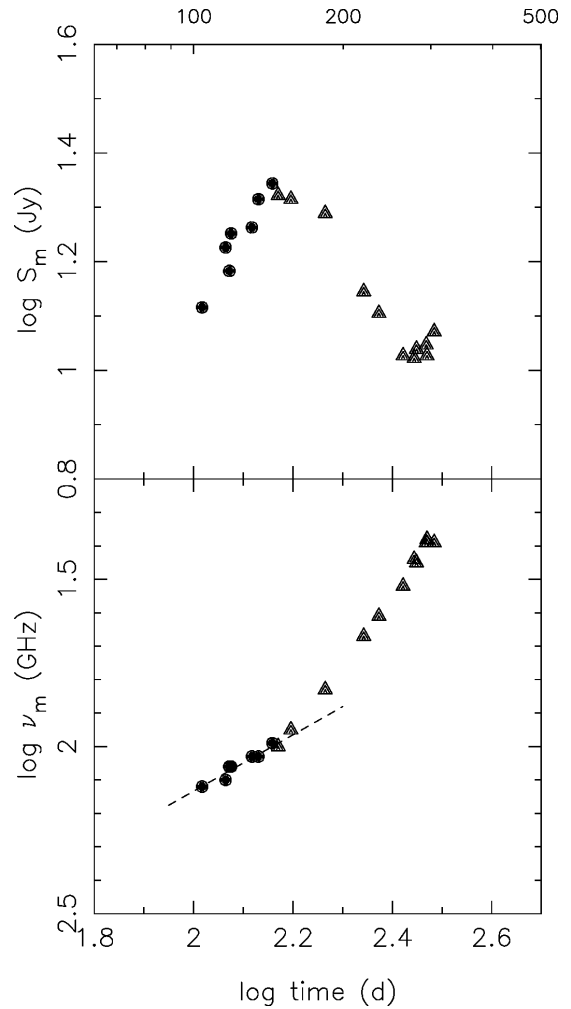


FIG. 8.—Evolution of the peak frequency (ν_m) and peak flux (S_m) with time. The dashed line on the lower panel “fits” the same eight points (*filled circles*) as in Fig. 7 and has a slope of -0.85 . The date of 1995 August 2 corresponds to time $t = 0$ (see text).

time. In order to determine the observational quantities necessary for comparison with theory, the spectra have been fitted as simple homogeneous synchrotron sources, i.e., with the equation

$$S_\nu = S_1(\nu/\nu_1)^{5/2} \{1 - \exp[-(\nu/\nu_1)^{-(s+4)/2}]\}, \quad (1)$$

where S_1 is a constant. The fitted spectra return the flux (S_ν) and frequency (ν_1) at the point where the optical depth reaches unity. The details of converting these values to peak flux (S_m) and peak frequency (ν_m) are given by, e.g., Stevens et al. (1995).

Because of the multicomponent nature of the spectra, only points indicated by filled symbols were included in the fits. This complicated spectral shape in the centimeter regime is almost certainly a result of the slow decay of the previous outburst. By 1996 March the 1995 flare dominates sufficiently for the entire spectrum to be represented by a single homogeneous component. The fitted parameters are given in Table 2, which also includes details of the third parameter determined by the fits, s , the index of an assumed electron injection spectrum. Column 1 has the date, column

2 the logarithm of the peak frequency, column 3 the logarithm of the peak flux, column 4 the electron parameter s , and column 5 the optically thin spectral index α .³ The values of s and hence of α are poorly determined, owing to lack of mid- to near-infrared data during the flare.

The fitted peak flux S_m is plotted against fitted peak frequency ν_m in Figure 7. The initial rise of S_m occurs between 1995 November 13 and 1995 December 27. From this date until 1996 February 1, S_m is approximately constant, and ν_m moves to lower frequency. After a gap in the coverage, both S_m and ν_m have decreased by 1996 March and continue to do so through 1996 April. Throughout 1996 May, S_m remains constant while ν_m moves slightly toward lower frequency. The dependences of S_m and ν_m on time can be followed by estimating the epoch at which the flare began ($t = 0$). This date is taken to be that of the last measurement immediately before the rise of the flare at the highest monitoring frequency giving 1995 August 2. Figure 8 shows that ν_m moves smoothly toward lower frequency with time. The dashed lines in Figures 7 and in the lower panel of Figure 8 are "fits" to the first eight points (*filled circles*) and give slopes of approximately -1.5 and -0.85 , respectively. The latter value is quite sensitive to the choice of epoch, $t = 0$. However, we note that the 90 GHz flux was already rising by 1995 August 25, and so, given that this frequency may lag the JCMT frequencies by about 20 days (§ 3.1), this date provides a firm upper limit. It is not possible to put similarly tight constraints on the earliest date for which $t = 0$, but for example, if $t = 0$ occurred either 2 weeks before or after 1995 August 2, then the respective indices are -0.75 and -0.95 . A detailed analysis of the evolution of the self-absorption turnover is given in § 4.

4. DISCUSSION

The analysis presented in the previous sections is now used to investigate the mechanisms responsible for the 1995 flare. A realistic model must successfully explain the three major observational results, namely the amplitude/lag relationship, the multifrequency polarization behavior, and the spectral evolution.

4.1. Spectral Evolution

As stated earlier, the flares in blazars are often attributable to relativistic shocks, and the only model that addresses the variability during the early stages of shock evolution is that of Marscher & Gear (1985). A brief summary of the model predictions follows.

The model consists of an adiabatic relativistic jet that is oriented toward the observer and contains transverse shock waves that form in response to changes in bulk flow or pressure. The magnetic field B in the jet is assumed to vary radially as a power law such that $B \propto R^{-a}$, where $a = 1$ for a magnetic field aligned perpendicular to the flow, and $a = 2$ for a parallel magnetic field. The evolution of the shock is described in terms of S_m and ν_m and is fixed at any one time by the dominant energy loss mechanism. When the emitting region is compact, inverse-Compton losses predominate (Compton stage), but these fall off rapidly with

radius as the shock expands and are superseded by synchrotron losses (synchrotron stage). As the shock expands further, the radiative lifetime of the electrons becomes large with respect to the time needed to traverse the emitting region, and losses caused by adiabatic expansion (adiabatic stage) become more important. Since electron radiative lifetimes are proportional to $\nu^{-1/2}$, the effective shock thickness is frequency dependent during the first two stages.

All three stages are approximated by power laws on the (S_m, ν_m) -plane. As the emitting region expands, ν_m is predicted to move to lower frequencies with time. S_m increases during the Compton stage, remains approximately constant during the synchrotron stage, and decreases during the adiabatic stage. The maximum flare amplitude for monitoring frequencies on the Compton stage occurs when the spectrum transits onto the synchrotron stage. Light curves at monitoring frequencies on the Compton stage are thus predicted to peak simultaneously, and because of the spectral shape, the flare amplitudes are expected to increase toward lower frequency. Flare amplitudes at monitoring frequencies commensurate with the later stages are determined by the details of the spectral evolution and are thus expected to be approximately constant during the synchrotron stage and to decrease during the adiabatic stage. Furthermore, such light curves will display time-lagged behavior with a delay between any two frequencies equal to the time taken for the spectrum to evolve between them and become optically thin. A detailed discussion of the flare lag/amplitude relation can be found in Valtaoja et al. (1992).

The flare amplitudes and time delays presented in Table 1 for the 1995 flare follow the predicted pattern very well. The amplitudes increase between 375 and 150 GHz, and no time delays were measured between the light curves at these frequencies. Between 150 and 90 GHz the amplitudes probably plateau, and there may be a small time lag between these wavelengths as found by Robson et al. (1993) for the 1987–1992 data streams. Below 90 GHz the light curves show increasing time delays with respect to the 270 GHz data, and the flare amplitudes fall off as expected.

The shape and evolution of the flare spectrum are also qualitatively consistent with the model (§ 3.3). Figure 7 shows all three phases of the predicted evolution: a steep rise of S_m with ν_m , possibly followed by a short-lived plateau stage, after which both S_m and ν_m fall as the spectral peak moves into the radio regime. The lower panel of Figure 8 shows the smooth progression of ν_m toward lower frequencies with time and is very similar in appearance to that for the 1991/1992 flare of 3C 345, which was modeled successfully as an adiabatically expanding shock (Stevens et al. 1996).

A detailed comparison with the model is possible for the rise of S_m with ν_m , which should correspond to the Compton stage. Marscher & Gear (1985) predict that

$$S_m \propto \nu_m^{-(11-a)/[2(a+1)]}, \quad (2)$$

and assuming that the radius of the jet R is proportional to time t ,

$$\nu_m \propto t^{-(a+1)/4}. \quad (3)$$

The 270 GHz polarization data discussed in § 3.2 indicate that the magnetic field was aligned along the jet axis during the early stages of the 1995 flare (see § 4.2), and so a value $a = 2$ is appropriate in this case. Equation (1) then gives

³ The electron energies are assumed to be distributed as $N(E) dE = kE^{-s} dE$, which leads to an optically thin spectral index $\alpha = (1 - s)/2$ above the break frequency where radiative losses are unimportant.

$S_m \propto v_m^{-1.5}$, and equation (2) gives $v_m \propto t^{-0.75}$, in excellent agreement with the observed dependences, which have indices of -1.5 and -0.85 , respectively (§ 3.3). The Compton stage should be accompanied by a steepening of the optically thin spectral index because of the frequency-dependent radiative losses suffered by the electrons in the shock. Unfortunately, although the fits of Figure 7 are of sufficient quality to pinpoint the turnover, lack of mid-IR data hinders an accurate determination of the spectrum at high frequencies. The model also predicts that high fluxes of X-rays and possibly of γ -rays should be associated with such a millimeter flare. These short wavelengths are predicted to lead the millimeter emission by about 1 month, but no data exist in the literature to verify this prediction, and unfortunately, the *X-Ray Timing Explorer* (XTE) did not produce data until after the flare peaked (I. M. McHardy 1997, private communication).

4.2. Polarization Behavior

The analysis so far supports the notion that the 1995 flare resulted from enhanced emission from a relativistic shock, but the interpretation of the polarization data is not so straightforward. The compression produced by a simple transverse shock will result in enhanced polarized flux if the magnetic field in the jet is largely tangled. The net magnetic field direction will be parallel to the shock front and thus perpendicular to the jet axis (Laing 1980). Alternatively, if the underlying jet has a significant component of magnetic field aligned parallel to the jet axis, as has been observed for several quasars (Cawthorne et al. 1993a, 1993b), then shock compression may lead to a *reduction* of the percentage polarization with no change in net magnetic field direction.

This latter effect is likely to occur in the jet of the quasar 3C 345, on scales coincident with the centimeter wavelength emission (Stevens et al. 1996), and, as was seen in § 3.2, also appears to hold for 3C 273 in the same wave band where flux and polarization are anticorrelated. Assuming optically thin radiation, the implied magnetic field direction is approximately parallel to the VLBI jet at all epochs. This assumption may at first sight appear unjustified, but note that the dominant contribution to both the total (from inspection of Figs. 1 and 6) and polarized flux (§ 3.2) comes from the underlying jet and occasionally from older, optically thin, radio components, rather than from the (initially) opaque new component.

At 270 GHz, however, the polarization behavior is inconsistent with both scenarios outlined above; the percentage polarization *increased*, and the polarization position angle remained orthogonal to the jet. Polarization measurements were made at two epochs during late 1995 (Nartallo et al. 1998), and on both occasions the spectra presented in Figure 6 show that the flux at this frequency was optically thin; therefore, the implied magnetic field direction must also be parallel to the jet. This magnetic field orientation, coupled with the observed increase of percentage polarization during the flare, is not readily produced by a transverse shock.

One possible, but unsatisfactory, interpretation is that a bend at the base of the jet contrives to produce an observed polarization position angle that is perpendicular to the jet, when in reality it is parallel. A second possibility is that the longitudinal component of the magnetic field at the base of the jet is enhanced by a pinch-mode instability that will also

produce the observed increase in intensity. However, it is difficult to envisage how such a scenario could result in the smooth evolution of the turnover from millimeter to centimeter wavelengths while closely following the predictions of the shocked-jet model. Instead, a more likely interpretation is suggested, in which the polarization and spectral variability are produced in a conical shock (Lind & Blandford 1985).

4.2.1. Conical Shocks

The polarization properties of conical shock waves have been modeled by Cawthorne & Cobb (1990), who show that both parallel and perpendicular polarizations can be produced. Net parallel polarization arises at small viewing angles (θ), for which relativistic beaming causes emission from the top (or bottom) of the cone to dominate over that from the sides. At larger θ , however, perpendicular E vectors from the sides of the cone just dominate over the parallel E vectors from the center. In such cases the degree of polarization cannot exceed about 10%, which is consistent with the observed maximum polarization of 6%–7% during the flare. Because of this beaming effect, a shock with a narrow cone angle will display a net perpendicular polarization over a larger range of θ than one with a broad cone angle.

The model also assumes that the magnetic field in the upstream plasma is tangled, which certainly appears to be the case at 270 GHz, given the minimum polarization of $0.72 \pm 0.13\%$ measured by Nartallo et al. (1998). Note that the correlation of polarization with flux at this wavelength (§ 3.2) rules out the possibility that this low value is a result of the magnetic field “cancellation” effect seen at 14.5 GHz.

Support for a conical shock model comes from a 22 GHz VLBI image of 3C 273 made in 1994 (Leppänen, Zensus, & Diamond 1995), a discussion of which follows. The component that is identified with the core has no detectable polarization to a limit of less than 0.5%, which, coupled with a similar lack of polarization at 5 GHz (Roberts et al. 1990), argues that the field at the base of the jet is tangled, rather than depolarized by Faraday rotation. For the component closest to the core, the polarization and total intensity maxima *coincide*, but at larger distances the polarization maxima occur *between* the knots. The magnetic field direction in the first knot is roughly parallel to the jet, and its polarization is only $\sim 3\%$. Finally, the parallel component of the magnetic field becomes stronger with increasing core distance, as found at 5 GHz (Roberts et al. 1990).

Leppänen et al. suggest that the data for each knot may be explained as cancellation of an underlying parallel magnetic field by transverse shocks of varying strength. The centimeter-wavelength single-dish polarization data presented here support their interpretation of magnetic field cancellation for the outer knots, although the shocks are not required to be transverse. The inner knot, however, is unlikely to be associated with a transverse shock, since the total and polarized intensities coincide, but with an implied magnetic field direction parallel to the jet.

Furthermore, an important conclusion from the results presented here is that both parallel and perpendicular magnetic field orientations are implied for the *same shock*, but at different frequencies, and thus, given the evolution of the flare spectrum with time, in different parts of the jet. A

suggested interpretation is that the shocks in the jet of 3C 273 are conical. At the base of the jet the conditions favor a shock with a cone angle that gives a parallel magnetic field, but further out in the jet the shock is disrupted by the growing parallel component of magnetic field, and its cone angle broadens, causing the polarization to flip by 90° . Alternatively, the same effect can be reached by allowing the inclination angle of the cone to change with respect to the observer's line of sight. Under certain conditions this variation need not be large. Inspection of Figure 3b of Cawthorne & Cobb (1990) shows that, for a cone angle of 10° , a maximum perpendicular polarization is reached for $\theta \sim 25^\circ$. However, if θ then becomes smaller by about 10° , then the polarization flips into a parallel orientation. Such "wiggles" in the jet have been observed in a VLBI map at 100 GHz (B   th et al. 1991).

It is also possible that future high-frequency VLBI observations could resolve such structures, in which case, for a net perpendicular polarization, higher degrees of polarization would be seen toward the edges (with E_\perp) and center (with E_\parallel) of the knot. Additionally, VLBI polarization monitoring data should show that a knot initially situated at the base of the jet will change its polarization properties as it expands outward. We predict that the polarization and total intensity maxima will initially be cospatial, and that the magnetic field at this point will be parallel, but sometime later, for the same knot the total intensity maximum will occur at a local minimum in polarized intensity. The magnetic field direction at this epoch will depend on whether the shock is sufficiently strong to dominate over the increasing component of magnetic field oriented parallel to the jet axis.

5. CONCLUSIONS

1. The flaring between 375 and 150 GHz is simultaneous, but time delays exist between these frequencies and the radio regime. The dependence of the lags with the flare amplitudes at the various monitoring frequencies follows the predictions of the shock model.

2. After separation of the variable and quiescent components, the flare spectra are well fitted as homogeneous synchrotron sources. The movement of the self-absorption turnover could thus be tracked during the outburst. The peak frequency evolved smoothly to lower frequencies with time, suggesting that the emitting region was expanding. During this period the turnover flux traced out the three stages predicted by the shock model of Marscher & Gear (1985). Good sampling of the rise phase of this spectral evolution allowed a detailed comparison with the model, and here the data are in excellent agreement with the pre-

dicted Compton stage. The production of X-rays during this outburst is thus a key question, but so far no data exist in the literature to verify the model prediction.

3. The polarization behavior during the outburst was found to be different at millimeter and centimeter wavelengths. For the latter regime the polarization monitoring data are consistent with the depolarization produced by a transverse shock as it propagates along a jet with a parallel magnetic field. However, the millimeter polarization properties are not consistent with such a structure. At 270 GHz (1.1 mm) the percentage polarization increases during the outburst, and the electric vector aligns across the milli-arcsecond VLBI jet, implying a parallel magnetic field orientation, since the radiation was optically thin. We thus observe different polarization behavior for the same shock, but, due to the observed lags, at different times. Since the time lags are produced by expansion of the emitting region along the jet, we thus observe different polarization behavior in different parts of the jet.

4. We suggest that the spectral and polarization data are consistent with a model in which a conical shock propagates along a "wiggling" jet that contains a largely tangled magnetic field at its base and a growing component of the magnetic field parallel to its axis. Such a shock can exhibit both parallel and perpendicular magnetic field orientations, and the transition from one state to the other may be caused by disruption of the shock owing to the growing magnetic field alignment in the underlying jet or to a change in viewing angle caused by a moderate bend in the jet.

Further modeling of the polarization properties of conical shocks propagating in different environments of magnetic field is encouraged. We would like to stress the importance of the multifrequency polarization observations to the correct theoretical interpretation of the outbursts in active galactic nuclei.

We thank Alan Marscher for reading and commenting on an earlier version of this paper. The James Clerk Maxwell Telescope is operated by the Joint Astronomy Centre in Hilo, Hawaii on behalf of the parent organizations PPARC in the UK, the National Research Council of Canada, and The Netherlands Organization for Scientific Research. The BIMA array is operated by the Berkeley Illinois Maryland Association with support from the National Science Foundation under grant AST 93-20238. M. F. A. and H. D. A. acknowledge support from NSF grant AST 94-21979. The observations from Mets  hovi are partly supported by the Finnish Academy of Sciences.

REFERENCES

- Aller, M. F., Aller, H. D., Latimer, G. E., & Hodge P. E. 1985, *ApJS*, 59, 513
 B   th, L. B., et al. 1991, *A&A*, 241, L1
 Cawthorne, T. V., & Cobb, W. K. 1990, *ApJ*, 350, 536
 Cawthorne, T. V., Wardle, J. F. C., Roberts, D. H., Gabuzda, D. C., & Brown L. F. 1993a, *ApJ*, 416, 496
 ———, 1993b, *ApJ*, 416, 519
 Cohen, M. H., Zensus, J. A., Biretta, J. A., Comoretto, G., Kaufmann, P., & Abraham, Z. 1987, *ApJ*, 315, L89
 Courvoisier, T. J.-L., Robson, E. I., Blecha, A., Bouchet, P., Hughes, D. H., Krisciunas, K., & Schwartz, H. E. 1988, *Nature*, 335, 330
 Duncan, W. D., Robson, E. I., Ade, P. A. R., Griffin, M. J., & Sandell, G. 1990, *MNRAS*, 243, 126
 Edelson, R. A., & Krolik, J. H. 1988, *ApJ*, 333, 646
 Gaskell, C. M., & Peterson, B. M. 1987, *ApJS*, 65, 1
 Gear, W. K., et al. 1994, *MNRAS*, 267, 167
 Hughes, P. A., Aller, H. D., & Aller, M. F. 1985, *ApJ*, 298, 301
 ———, 1989a, *ApJ*, 341, 54
 ———, 1989b, *ApJ*, 341, 68
 Laing, R. A. 1980, *MNRAS*, 193, 439
 Lepp  nen, K. J., Zensus, J. A., & Diamond, P. J. 1995, *AJ*, 110, 2479
 Lichti, G. G., et al. 1995, *A&A*, 298, 711
 Lind, K. R., & Blandford, R. D. 1985, *ApJ*, 295, 358
 Litchfield, S. J., Robson, E. I., & Hughes, D. H. 1995, *A&A*, 300, 385
 Marscher, A. P., & Gear, W. K. 1985, *ApJ*, 298, 114
 McNaron-Brown, K., Johnson, W. N., Dermer, C. D., & Kurfess, J. D. 1997, *ApJ*, 474, L85
 Nartallo, R., Gear, W. K., Murray, A. G., Robson, E. I., & Hough, J. H. 1998, *MNRAS*, in press

- Peterson, B. M. 1993, *PASP*, 105, 247
Roberts, D. H., Kollgaard, R. I., Brown, L. F., Gabuzda, D. C., & Wardle, J. F. C. 1990, *ApJ*, 360, 408
Robson, E. I., et al. 1983, *Nature*, 305, 194
———, 1993, *MNRAS*, 262, 249
Stevens, J. A., Litchfield, S. J., Robson, E. I., Cawthorne, T. V., Aller, M. F., Aller, H. D., Hughes, P. A., & Wright, M. C. H. 1996, *ApJ*, 466, 158
Stevens, J. A., Litchfield, S. J., Robson, E. I., Gear, W. K., Teräsrananta, H., Tornikoski, M., & Valtaoja, E. 1995, *MNRAS*, 277, 1146
Stevens, J. A., Litchfield, S. J., Robson, E. I., Hughes, D. H., Gear, W. K., Teräsrananta, H., Valtaoja, E., & Tornikoski, M. 1994, *ApJ*, 437, 91
Stevens, J. A., & Robson, E. I. 1994, *MNRAS*, 270, L75
Teräsrananta, H., et al. 1992, *A&AS*, 94, 121
Ulich, B. L. 1981, *AJ*, 86, 1619
Unwin, S. C., Cohen, M. H., Biretta, J. A., Pearson, T. J., Seielstad, G. A., Walker, R. C., Simon, R. S., & Linfield, R. P. 1985, *ApJ*, 289, 109
Valtaoja, E., Teräsrananta, H., Urpo, S., Nesterov, N. S., Lainela, M., & Valtonen, M. 1992, *A&A*, 254, 71